PHYSICAL REVIEW B VOLUME 31, NUMBER 6 15 MARCH 1985

Surface-enhanced Brillouin scattering on silver films

A. L. Moretti, W. M. Robertson, B. Fisher,* and Ralph Bray
Department of Physics, Purdue University, West Lafayette, Indiana 47907
(Received 15 October 1984)

We report the first observation of surface-enhanced Brillouin scattering involving the intimate interaction of the extended surface-plasmon (SP) polaritons of a silver film on a glass substrate with the thermal-equilibrium surface acoustic waves of the film. The role of the SP in the Brillouin scattering process is demonstrated and analyzed for a particular optical configuration, specifically, SP generation in the attenuated-total-reflection Kretschmann geometry, with Brillouin scattering observed on the air side of the silver film. Good agreement is obtained between theory and experiment, both in the form of the resonance in the Brillouin scattering signal and in the magnitude of the enhancement by the SP.

I. INTRODUCTION

Surface-plasmon (SP) polaritons play a central role in a host of interesting surface-enhanced, nonlinear optical phenomena which have been intensively studied in recent years, e.g., surface-enchanced Raman scattering[1] (SERS) from adsorbed chemical species, and second-harmonic generation (SHG).[2–5] Much of the enhancement is attributed to the increased electric fields associated with SP at the metal surfaces, particularly silver. The magnitude of the enhancement and the analysis of the SP interaction is very much a function of the structure of the surface.[6] The enhancement can be extraordinarily large[1] ($>10^6$) for the case of silver-island films deposited on substrates or electrochemically roughened silver surfaces, where the SP's are localized in nature, but rather modest (<100) (Refs. 2, 6, and 7) for "smooth" silver surfaces, where the SP's are extended in nature.[6,8,9] In the phenomena cited above, the enhancement can also be strongly dependent, directly or indirectly, on the particular chemical adsorbate.[1,5]

In this paper we shall describe our effort to add Brillouin scattering from acoustic waves at the surfaces of metals to the list of SP-enhanced phenomena. We report here the first demonstration of surface-enhanced Brillouin scattering (SEBS), for the thermal-equilibrium surface acoustic waves (SAW) of smooth silver films deposited on a glass substrate. The enhancement was obtained utilizing the extended SP polaritons, generated by the attenuated-total-reflection (ATR) Kretschmann method,[9,10] at the silver-air interface. The magnitude of the enhancement ($\sim 25\times$) was determined and compared with theory, using parameters for the complex dielectric constant ϵ_{Ag} of silver derived from the analysis of the resonant interaction of the SP and the acoustic waves. The success of these studies will be contrasted with the failure to observe any significant Brillouin scattering enhancement for the case of silver-island films, with their localized SP, deposited on a GaAs substrate.

A theoretical prediction of the feasibility and magnitude of SEBS for thermal phonons interacting with extended SP was presented by Fukui *et al.*[11] However, there has been no previous experimental determination of the enhancement factor. Earlier, the interaction between extended SP's and phonons had been demonstrated by Talaat *et al.*,[12] for transduced, low-frequency SAW, but with no determination of the enhancement *per se*. These experiments were analyzed later by Talaat *et al.*,[13] and in more detail by Marvin *et al.*[14] Although the latter analysis does not deal with thermal phonons, it has provided a most useful base for the analysis of the work to be presented here because it is applicable to a light-scattering configuration which we found to be most feasible to implement experimentally.

II. CONCEPTS IN THE DESIGN OF THE EXPERIMENTS

For the discussion of the design of the experiments and the analysis of SEBS, a number of interesting concepts need to be reviewed. We shall consider below the nature of surface Brillouin scattering as distinguished from bulk Brillouin scattering, and why it is necessary to use the former to study the interaction of SP's with phonons. We shall describe the several forms in which the interaction between SP's and phonons can be manifested, and then discuss in detail the one we found to be most suitable for analyzing SEBS.

A. The nature of surface Brillouin scattering

Surface Brillouin scattering is distinguished from bulk Brillouin scattering by the depth of interaction of the light with the phonons, and not by the nature of the phonons (whether surface or bulk) participating in the interaction. The very limited depth of interaction which characterizes surface Brillouin scattering can be achieved in a number of ways, e.g., by the high opacity of the material[15] as in the case of metals, by the depth of the acoustic waves (about an acoustic wavelength) in the case of SAW, and by the possible surface nature of the light-scattering mechanism itself.[16,17] An example of the last case is the ripple scattering mechanism[16–18] due to the corrugations generated on the surface by the vibrations of the atoms.

This is the predominant surface scattering mechanism, not only for SAW, but also for bulk phonons striking the surface. In all these cases of very limited depth of interaction, Brillouin scattering is governed by a relaxed wave-vector conservation law similar to that for a surface grating, i.e., only the components of wave vector parallel to the surface are conserved. Surface Brillouin scattering is then operationally identifiable by its adherence to this relaxed conservation law. This is manifested by a very broad spectrum for the scattering contribution from bulk phonons.[18] At a given scattering angle, bulk phonons with a specific wave-vector component in the surface have a wide range of components of wave vector normal to the surface, and hence a broad range of frequencies. They thus generate a continuum contribution to the Brillouin spectrum. However, for SAW, a sharp-line Brillouin spectrum is obtained because their frequencies are determined uniquely by their wave vectors which lie completely in the surface. The more familiar bulk Brillouin scattering involves an in-depth interaction with the bulk phonons, which requires full conservation of wave vector, and hence yields a sharp-line spectrum.

Since SP's are characterized by enhanced electric fields which peak strongly at the metal-air surface,[10,11] only surface scattering phenomena can be fully affected and enhanced. Thus surface Brillouin scattering is eminently suited for studying the enhancement due to SP. Although SAW provide the easiest regime for such studies, the very broad surface Brillouin spectrum obtainable for bulk phonons at the surface, as alluded to above, should also be capable of fully demonstrating SP enhancement.[11] However, because of the nature of the SP, bulk Brillouin scattering can be enhanced only partially, and the enhancement factor would be very difficult to determine.

B. The SP generation method

For a discussion of the means for generating SP's, we refer to the dispersion curve for extended SP's, as schematically illustrated in Fig. 1. The SP's are characterized by a frequency ω_{SP} and a well-defined wave vector $\mathbf{k}_{SP}$ in the surface of the metal. Direct coupling between photons and the extended SP is not possible. The light line in air does not cross the SP dispersion curve, and hence cannot fulfill the requirements of frequency and wave-vector conservation. At best, for glancing angle of incidence, it is parallel to the base of the SP dispersion curve. However, coupling can be achieved by various techniques. For example, a grating[19] formed on a metal surface can supply the additional parallel wave-vector component to augment that of the incident light to achieve coupling to the SP. In the same way, inherent surface roughness[20] (equivalent to a superposition of gratings) or phonons[13] (as propagating gratings), can also promote coupling. In the present experiment we make use of a very well known and convenient technique, the attenuated-total-reflection (ATR) Kretschmann geometry,[9,10] which is illustrated in Fig. 2(a). A thin silver film is vacuum deposited on the flat side of a glass hemisphere. A laser beam, incident at angle θ_i through the glass, is focused at the silver film. For p-polarized light, SP's are resonantly generated on the metal-air interface at that incident angle of light, θ_{SP}, at which the surface wave-vector component of the light (increased by the index of refraction of the glass) matches that of the SP. This is represented in Fig. 1 by the intersection of the light line in the glass with the SP dispersion curve. The resonant generation of SP's is matched by a sharp, resonant decrease in the reflected light,[10] as illustrated in

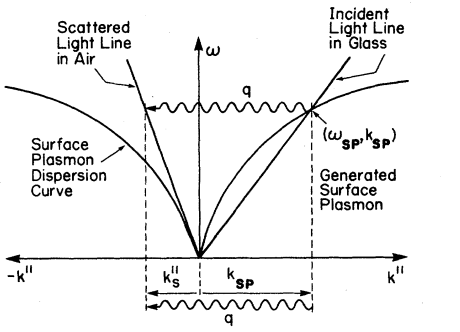

FIG. 1. Dispersion curve illustrating SP generation in the ATR Kretschmann geometry and subsequent phonon interaction. The SP's are generated when the light is incident through a glass prism on a silver film. The surface-enhanced Brillouin scattering occurs when the SP radiate into the air with the assistance of a phonon of wave vector q.

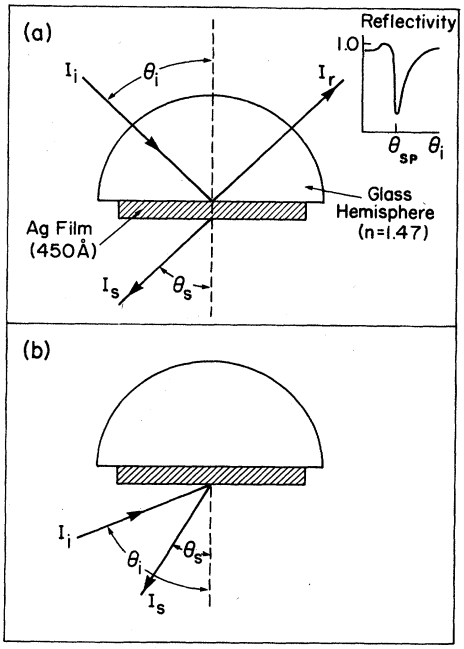

FIG. 2. (a) The ATR Kretschmann configuration used to generate the SP's. Light is incident through a glass hemisphere ($n=1.47$) onto a thin, vacuum-deposited silver film ($h=450$ Å). The resonant generation of the SP's at the incident angle θ_{SP} is manifested by a sharp drop in the reflected light. The scattered light is observed on the air side at the angle θ_s. (b) The external reflection (ER) configuration is used for Brillouin scattering without SP participation on the same silver film. The light is both incident and scattered on the air side.

the inset in Fig. 2(a). The resonant angle is a function of the frequency of the incident light.

C. SP interactions with surface phonons

We turn next to the interaction of SP's with phonons, and how this is manifested in the Brillouin spectrum. The SP-phonon interaction can occur in several ways.[13]

Case (1). The SP generated by the ATR technique can be scattered into another SP, either inelastically by phonons or elastically by roughness. The wave vectors of the scattered SP must terminate on a circle of essentially constant wave vector in the plane of the film. The scattered SP can couple back into photons through the glass prism by the reverse ATR Kretschmann mechanism. The emergent scattered light must lie on the surface of a cone,[21,22] of angle θ_{SP}. The backscattering configuration of this interesting case is the one theoretically analyzed by Fukui *et al.*[11] However, it is the most difficult to implement experimentally. We have observed that its dominant contributions in the Brillouin spectrum come from the strong bulk Brillouin scattering in the glass hemisphere itself, and that these contributions can obscure the surface scattering signal in which we are interested. The competition between the bulk and surface contributions are eliminated in case (2), and we have therefore focused our attention and report here only on that case.

Case (2). SP's are generated in the same manner as in case (1), from light incident at the resonant angle on the glass hemisphere. Now, however, the originally generated SP's use the interaction with phonons (or roughness) to directly couple out as light on the air side of the metal film as shown in Fig. 2(a). We illustrate in Fig. 1 how a surface wave vector q, supplied by the appropriate phonon, facilitates the coupling of the SP out as photons on the air side of the silver film. The angle at which the light is emitted, θ_s, is then a function of the wave vector of the participating phonon. Here, the bulk Brillouin scattering contributions from the phonons in the glass hemisphere are so strongly attenuated in passing through the silver film, that they become unobservable in the spectrum obtained on the air side. This greatly simplifies the study of the surface Brillouin spectrum of the silver film.

Case (3). A final possibility is the reverse of case (2). The interaction of light incident on the air side of the silver film, with phonons in the silver, can be used to couple that light into SP's in the metal. The SP's can then radiate out as light through the glass prism.

We have observed all three forms of the SP-phonon interaction. In every case the radiated light, when analyzed by a Fabry-Perot interferometer, shows the frequency-shifted Brillouin couplet. However, these cases are not all equally suited for attaining the major objectives of this study, which are (i) the demonstration of the resonant behavior of the SEBS of the thermal SAW, and (ii) the determination of the SP enhancement factor.

The relevant conditions for Brillouin scattering in case (2) are given by

$$\mathbf{k}_s^{\parallel}=\mathbf{k}_{SP}\pm\mathbf{q}, \quad \text{and } \omega_s=\omega_{SP}\pm\omega_q\ , \tag{1}$$

where $\mathbf{k}_s^{\parallel}$ and ω_s are the surface wave-vector component and frequency of the scattered light, and $\mathbf{k}_{SP}$ and ω_{SP} are the SP wave vector and frequency. The SAW wave vector $\mathbf{q}$ is related to its frequency by $\omega_q=qv$, where v is the surface acoustic velocity. In the more usual external reflection (ER) configuration [Fig. 2(b)], where there is no SP involvement, the $\mathbf{k}_i^{\parallel}$ and ω_i for the incident light replace $\mathbf{k}_{SP}$ and ω_{SP} in Eq. (1).

III. EXPERIMENTAL DETAILS

The heart of the experimental system is a computer-stabilized, five-pass Fabry-Perot interferometer[23] with a contrast ratio of $\sim 10^9$. It is fully capable of giving the enhanced and unenhanced Brillouin spectra.

The experimental arrangement used for the Brillouin scattering measurements is illustrated in Fig. 3. Light from a single-moded argon-ion laser ($\lambda=4880$ Å) is brought to sample elevation by the periscope P. Right-angle scattering is used for the ATR configuration. The incident light is directed by the lens L_1 along the radius of the glass hemisphere[24] (index of refraction $n=1.47$), where it is tightly focused onto the silver film. The hemisphere is mounted on a rotating table, whose axis of rotation coincides with the silver film. The collection lens L_2 collimates a portion of the scattered light, which then passes through the spatial filter defined by L_3, the front pinhole (FPH) and L_4. The scattered light beam is frequency-analyzed by the five-pass Fabry-Perot interferometer. The output beam is sent through another spatial filter formed by L_5, the rear pinhole (RPH) and L_6, which focuses it onto the photocathode of a cooled ITT FW 130 photomultiplier tube (PMT) after passing through a 10-Å bandwidth interference filter (IF). A solenoid actuated filter can be moved into the focused

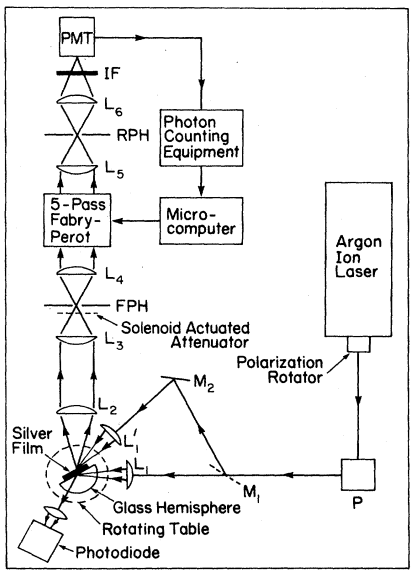

FIG. 3. Brillouin scattering setup with computer-controlled, five-pass Fabry-Perot interferometer. M represents mirrors; L, lenses; P, a periscope; FPH and RPH represent the front and rear pinholes; IF, an interference filter; PMT, a photomultiplier tube.

beam just before the FPH to attenuate the collected light when the interferometer scans through intense features in the spectrum. With careful alignment the incident beam will not walk across the silvered face of the hemisphere when the sample is rotated, keeping the scattered light spot in the field of view of the interferometer as defined by the collection optics. This is not possible with a prism. The reflected beam intensity is determined before and after a Brillouin scattering run by measuring the voltage across a photodiode when the chopped reflected light is focused onto its photocathode.

The sample was rotated to vary θ_i through the resonant angle θ_{SP} at 46°10′. For convenient right-angle scattering, θ_s is in the vicinity of 44°, and we observe Rayleigh SAW of ~ 6 GHz.

The input optics can be changed to the ER configuration by accurately positioning mirror M_1, which is mounted on a precision micrometer-driven translation stage, in the laser beam after P. The light is reflected off mirror M_2 and focused onto the air side of the silver film by lens L_1'. The angles used here to observe phonons close to 6 GHz are $\theta_i = 78°$ and $\theta_s = 48°$. The system can be switched between the two configurations with no realignment by translating M_1 in and out of the incident laser beam.

The PMT is set up for photon counting, with the counts being collected by a microcomputer system. The microcomputer not only displays and accumulates the spectrum, it is part of a feedback system which is capable of maintaining the optical alignment of the interferometer indefinitely. For the experiments discussed here, it was generally sufficient to accumulate 500 sweeps with scan times of 2 s each.

The silver films are evaporated onto the flat, polished side of the glass hemisphere in a vacuum of $\sim 10^{-6}$ Torr at a rate of 1–2 Å/s. A silver film thickness $h = 450$ Å was empirically found to optimize the generation of SP on the silver-air interface at the selected wavelength.

IV. RESULTS AND ANALYSIS

A. Nature of the SAW and the Fabry-Perot scans

For thin films on a bulk substrate, as for the present situation, there are two types of surface waves with transverse vibrational components that can generate surface ripples: the Rayleigh waves and the higher-order modes, called Sezawa waves,[25] which propagate at higher velocities. The ripples on both interfaces can contribute to the Brillouin scattering signal.[14] The interference between these two contributions will be opposite in character for the two types of waves because of the differences in the symmetry of the vibrations. The velocities of both types of waves are dependent on the parameter hq, which is $\simeq 1$ in the present experiments. The velocity of the Rayleigh waves[25] of the film is intermediate between that of the Rayleigh waves of bulk silver and the glass substrate. In spectra taken with suitable free spectral range, we have been able to see both the Rayleigh and the first Sezawa waves. Such a spectrum is shown in Fig. 4 for the enhanced case. The large truncated peak is due to the parasitic, elastically scattered light and the large, sharp peaks on either side correspond to the Stokes and anti-Stokes components of the Brillouin scattered light for the Rayleigh waves. The Brillouin couplet for the Sezawa waves is visible at much higher frequency shifts, and its intensity is much weaker than for the Rayleigh waves, but it is nevertheless quite distinct. We shall restrict all further discussion and analysis to the much stronger Rayleigh wave signals.

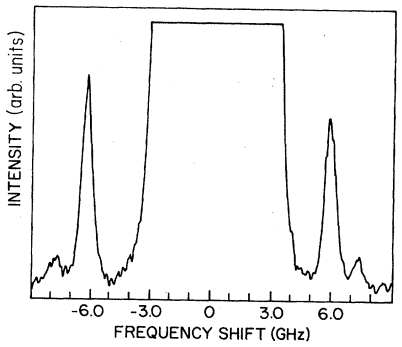

FIG. 4. Five-pass Fabry-Perot interferometer scan showing the SP-enhanced Brillouin scattering spectrum of both the strong Rayleigh (6 GHz) and weak Sezawa waves. The Sezawa waves are from overlapping orders in the Fabry-Perot scans and are at 10.1 GHz. The large truncated peak is due to the elastically scattered light.

B. The resonant character of SEBS: comparison of theory and experiment

The results of simultaneous studies of the angular dependence of the reflectivity and of the Brillouin scattering for case (2) of Sec. II C are shown in Figs. 5(a) and 5(b), respectively. Just as the minimum in the reflectivity in the ATR configuration [Fig. 2(a)] is a demonstration of the resonant generation of SP's at the incident angle θ_{SP}, a resonant peak in the Brillouin scattering signal at the same angle is a demonstration of its dependence on SP interaction. A similar resonance is also obtained for the elastically scattered light [Fig. 5(c)]. When the above measurements are repeated with s-polarized incident light, no SP generation can occur, and indeed no resonant behavior is observed. The solid curves in Fig. 5 are theoretical fits based on the analysis described below.

Our analysis of the Brillouin scattering resonance is based on the theory presented by Marvin *et al.*[14] It entails the solution of Maxwell's equations with boundary conditions imposed by the glass-metal and metal-air interfaces. The phonon involvement is expressed by introducing sinusoidal ripples of amplitude u_g and u_a at the glass and air boundaries of the silver film. Since scattering from thermal phonons deals with a distribution of phonon frequencies determined by the collection optics, these amplitude parameters represent a root-mean-square value. For a sufficiently thin film, with the parameter $hq \sim 1$, it is expected that the vibrational amplitudes on the two interfaces are correlated, and that there is interference of the light scattered from the two surfaces. In that case, the

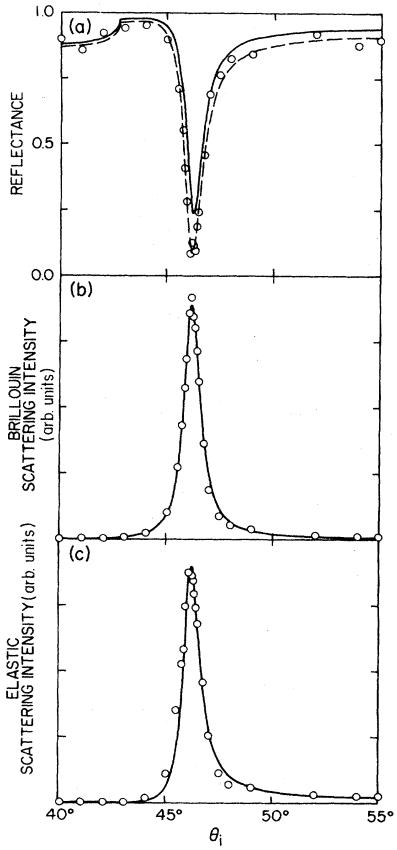

FIG. 5. Resonant curves for (a) reflectivity, (b) Brillouin scattering, and (c) elastic scattering, taken as a function of the angle θ_i for light, at 4880 Å, incident through the glass hemisphere onto the silver film. The sharp peaks in (b) and (c) at $\theta_{SP}=46°10'$ are coincident with the reflectivity minimum in (a), demonstrating a mutual resonant dependence on SP generation. The solid curve in (b) is a theoretical fit, yielding $\epsilon_{Ag}=-8.9+0.27i$. The solid curves in (a) and (c) are theoretical plots using this value of ϵ_{Ag}. The dashed curve in (a) is based on an independent theoretical fit to the reflectivity, which gives $\epsilon_{Ag}=-9.0+0.43i$.

scattering cross section [Eq. (4b) of Marvin *et al.*[14]] can be expressed in the form

$$\langle\,|\,Au_a-Bu_g\,|^2\rangle=\langle A^*Au_a^2\rangle+\langle B^*Bu_g^2\rangle-\langle 2\,\mathrm{Re}(A^*B)u_au_g\rangle\,, \tag{2}$$

where A and B are functions of h, θ_i, θ_s, the dielectric constant of the glass, and the complex dielectric constant of silver $\epsilon_{Ag}=\epsilon'+i\epsilon''$.

The first term on the right-hand side of Eq. (2) represents the time-averaged scattering intensity for ripples at the metal-air interface, the second term is for ripples at the glass-metal interface, and the last term is for the interference of the light scattered at the two interfaces. Since the SP electric fields peak strongly at the metal-air interface, the SP resonance affects mainly the scattering from that boundary. The resonant peak is therefore determined mainly by the $\langle A^*Au_a^2\rangle$ term. The resonant angle is determined primarily by the real part of the dielectric function ϵ', and the angular half-width of the peak by the imaginary part ϵ''. Finally, sufficiently far away from resonance, all three terms in Eq. (2) become comparable. There the wings of the resonant peak should yield information on the relative ripple amplitudes $\beta=u_g/u_a$ and on the interference between their scattering contributions.

Values of ϵ_{Ag} and β can be obtained by using them as the variable parameters in a least-squares fit of the theory to the data. A very good fit to the Brillouin resonance data alone is shown by the solid curve in Fig. 5(b), for values of the parameters given by $\beta=1.1$ and $\epsilon_{Ag}=-8.9+0.27i$. The same value of ϵ_{Ag} also gives a very good fit to the resonance of the elastic scattering data in Fig. 5(c). However, its application in the analysis of the reflectivity dip [solid curve in Fig. 5(a)] gives only a fair fit there. A better fit to the reflectivity is obtained for a value of $\epsilon_{Ag}=-9.0+0.43i$ as shown by the dashed curve.

This analysis suggests that there may be some incompatability, particularly in the fitted values of ϵ'', between the resonant reflectivity and Brillouin scattering data. This may be due to systematic experimental error, but it is also possible that the theories are too idealized in assuming a smooth surface with a small perturbation due only to phonon-induced ripples. Prior studies[20] have shown that roughness can have profound effects on the SP dispersion curve and the resonant reflectivity peak. Such effects are empirically expressed in an effective value of ϵ_{Ag}. It is not clear that the effective value of ϵ_{Ag} obtained for one type of measurement (e.g., reflectivity) is valid for other types of measurement (e.g., Brillouin scattering). In any event, we cannot take the discrepancy in ϵ'' too seriously since similar measurements, made on several different silver films, gave a spread of values for ϵ'' in the range 0.2 to 0.7. This spread indicates that the value of ϵ'' is sample sensitive, probably dependent on film roughness and aging. The data in the literature[26] for this parameter, from a variety of different types of measurements, give an even wider spread of values.

C. Interference effects between the two interfaces

The parameter β is also sensitive to the value of ϵ_{Ag} used in fitting the Brillouin resonance data, and we therefore have no great confidence in the value quoted. Nevertheless, interesting insight can be extracted from the theory of Eq. (2), about the interference between the scattering contributions of the phonon-induced ripple amplitudes u_g and u_a on the two silver interfaces. The results of such an analysis are shown in Fig. 6, where a series of theoretical plots are presented for the specific values of $\beta=0$, 1, and 2, representing increasing ripple amplitude u_g on the glass side, for a fixed amplitude on the metal-air side. The resonant peak is obviously not greatly sensitive to u_g; it decreases slightly with increase in u_g. However, varying u_g does have an interesting effect on the wings of the resonant peak. Increasing u_g from zero, increases the signal on the left side of the peak, but decreases the signal on the right side, thus revealing that there is a transition from constructive to destructive interference of the two contributions. The transition occurs just below θ_{SP}. (See *Note added in proof.*)

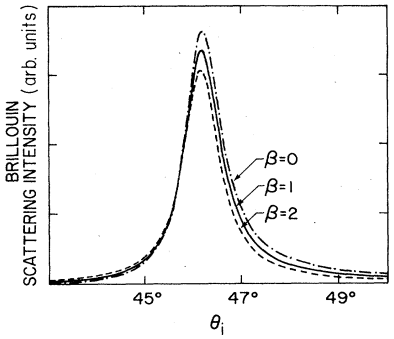

FIG. 6. Theoretical Brillouin scattering resonance curves for varied values of $\beta=\mu_g/u_a$, the relative ripple amplitudes on the glass and air interface. The crossover of the curves shows the transition from constructive to destructive interference at θ_i just below θ_{SP}.

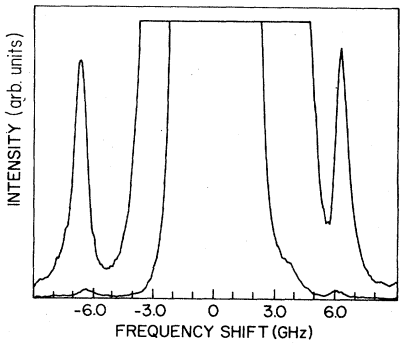

FIG. 7. Determination of the magnitude of the SP enhancement of Brillouin scattering. Comparison of a five-pass Fabry-Perot interferometer scan of SP-enhanced Brillouin scattering components of thermal equilibrium SAW in the Kretschmann configuration (upper curve) with an unenhanced spectrum (lower curve) in the external reflection configuration where no SP's are involved.

D. Determination of the SP-enhancement factor

How to determine the SP enhancement for Brillouin scattering is not immediately obvious; there are some pitfalls to watch out for. For example, it may be tempting to take the relative height of the resonant peak with respect to the off-resonance wing in Fig. 5(b) as a measure of the SP enhancement. However, this approach is very misleading. It gives an enhancement factor that is excessively large ($\gg 100\times$). It does not take into account the fact that the off-resonance contributions from both sides of the metal film are unduly weak because they are both attenuated strongly in passing through the silver film. A more reasonable approach is to compare the peak resonant Brillouin signal with the nonresonant signal in the ER configuration. The peak resonant signal represents predominantly the signal for the SP-enhanced scattering from the metal-air interface. The ER signal is primarily due to the unenhanced scattering signal from the same interface, since the contribution from the glass-metal interface undergoes double attenuation in the silver film.

In Fig. 7 we present just such a comparison for two interferometer scans taken for acoustic phonons of almost the same frequency by suitable selection of the pair of incident and scattering angles (θ_i,θ_s). For the enhanced case, θ_i is necessarily fixed at θ_{SP} by the condition for SP generation. The acoustic frequency is then uniquely determined by θ_s. For the ER case, there is wide latitude in choosing a pair of angles that will be appropriate for the given acoustic frequency. We chose that pair which gave the maximum signal according to ripple scattering theory.[18] Since the strengths of the peaks are quite sensitive to the optical alignment of the whole system, particularly the Fabry-Perot interferometer, and to the success in finding the maximum of the SP resonance (by monitoring the minimum in the reflectivity peak), a series of measurements were made, going back and forth between the two configurations. In this manner we obtained an average enhancement factor of $25\pm25\%$.

Two corrections had to be made in order to determine the enhancement factor. (i) In the ATR case it is necessary to use much smaller incident power (<30 mW focused to ~ 75 μm average diameter spot size) to avoid damaging the silver film. Normalization for incident power is included in the comparison of the spectra shown in Fig. 7. (ii) Depending on the size of the pin holes chosen for the Fabry-Perot interferometer, not all of the incident light spot on the metal may contribute to the scattered light ultimately collected. Since the size and shape of the incident light spot are different in the two configurations, a correction was required which served to reduce the enhancement obtained from the raw data.

As can be seen in Fig. 7, the elastically scattered signal is also very strongly enhanced. A quantitative determination of the enhancement factor for the latter is much more difficult to establish because the parasitically scattered light is quite variable from point to point on the surface, and it is not certain that comparative measurements are being made on the same point in the two types of measurements.

It is often stated that the enhancement factor can be obtained from the increase in the electric field of the SP over that of the incident field in vacuum. For the experiment reported here, we calculate a field increase of ~ 10, suggesting an enhancement of ~ 100. However, this simple approach may not take into account all the factors that contribute to the enhancement. We therefore resort to the theory of Marvin *et al.*[14] to calculate the enhanced Brillouin scattering intensity for the configuration of case (2) in Sec. II C. A modification of this theory was used to also extract the unenhanced scattering intensity in the ER geometry. Using our experimental values for incident and scattering angles, and the value of ϵ_{Ag} determined from fitting the theory to the Brillouin resonance data, we calculate an enhancement factor of 25, in excellent agreement with the average, measured value. When using the somewhat different value of ϵ_{Ag} determined from the fit to the reflectivity curve, an enhancement of 20 is obtained, which is still within the variation limits of the measured values. The calculated value of the enhancement factor is not sensitive to the value of β, since the ripples at the glass interface do not contribute significantly to the scattering in either the enhanced or unenhanced case.

Finally, it should be noted that the enhancement factor determined in the above discussion relates only to the surface-plasmon–phonon interaction of case (2) in Sec. II C. The enhancement factor could be quite different for the other cases.

V. ABSENCE OF ENHANCEMENT FOR SILVER ISLAND FILMS

The enhancement seen in the case of extended SP's is in contrast to the failure to see significant enhancement for the case of localized plasmons characteristic of roughened surfaces or metal islands (where SERS and SHG demonstrate huge enhancements). We looked for enhanced Brillouin scattering due to silver islands, of mass thickness 50–100 Å, deposited on one part of a GaAs substrate. We observed sharp Brillouin peaks from the SAW of GaAs on both the bare region of the substrate surface and on the silver-island region. The enhancement in the latter case was negligible, despite the fact that the deposited islands were found to be SERS active for adsorbed monolayers of *p*-nitrobenzoic acid. There was, however, a huge increase both in the elastically scattered light and in the base of the Brillouin spectrum. We attribute the failure to observe enhancement of the sharp-line Brillouin couplet to the fact that wave vector is undefined for localized SP's. Hence, a very broad portion of the frequency spectrum of the thermal acoustic phonons may be able to contribute to the scattering signal at any angle of observation. This can manifest itself only as an enhanced broad background, overlapping many orders in a Fabry-Perot interferometer scan with limited free spectral range.[27] This difficulty would not be applicable to SERS, where the Raman spectrum inherently consists of discrete lines.

VI. SUMMARY AND CONCLUSIONS

We have successfully demonstrated the role of extended surface-plasmon (SP) polaritons in promoting surface-enhanced Brillouin scattering (SEBS). The SP's were generated in the ATR Kretschmann configuration, on a smooth silver film deposited on the flat surface of a glass hemisphere, and were scattered by the thermal equilibrium surface acoustic waves (SAW) of the silver film. The scattered light was analyzed on the air side of the film by a five-pass Fabry-Perot interferometer. An important factor in the design of the experiment was the need to obtain an intimate interaction between the phonons and the enhanced electric fields of the SP's, which are strongly peaked at the metal-air interface. The desired intimacy was ideally achieved in the present interaction, since the predominant mechanism of scattering by the SAW involves the propagating ripples that the phonons generate at the surface. Sharp-line Brillouin couplets were seen for the Rayleigh and first Sezawa waves in the interferometer scans.

Resonant generation of SP's is obtained by appropriately varying the angle at which the laser beam is incident through the glass hemisphere onto the silver film. A resonant peak was obtained in the Brillouin scattering intensity which coincided with a resonant dip in the reflectivity and a resonant enhancement of the parasitic scattering signal, demonstrating the mutual involvement of all three phenomena with the resonant generation of SP's. A measure of the SP enhancement factor for a particular SP-SAW interaction [case (2) of Sec. II C] was obtained by comparing the peak-enhanced Brillouin scattering intensity from phonons on the silver-air interface, with the unenhanced intensity from the same phonons in an external reflection geometry.

The resonant Brillouin scattering was analyzed by the theory of Marvin *et al.*,[14] in terms of the fitted parameters ϵ_{Ag} of the silver film and the ratio of the ripple amplitudes β, on the two interfaces (glass and air) of the silver film. The absolute values of the ripple amplitudes were not determined. Quite good fit to the form of the resonance was obtained. The fitted parameters were found to be strongly sample dependent, presumably reflecting differences in roughness and aging of the films. With use of the fitted value for ϵ_{Ag} of the silver film, the magnitude of the enhancement factor was calculated, and it agreed very well with the experimentally determined value of 25.

Note added in proof. After the completion of the present analysis, the relative ripple amplitude β was theoretically calculated by F. Nizzoli on the basis of the acoustical model presented in Ref. 25. For the specific conditions of our experiment (6-GHz SAW in a 450-Å silver film on a glass substrate), he obtained a value for β of 1.04. We gratefully acknowledge his communication to us of this result.

ACKNOWLEDGMENT

The work was supported by the National Science Foundation through the Materials Research Laboratory Grant No. DMR-80-20249, and equipment support from Grant No. 82-17442.

*Present address: Department of Physics, Technion, Haifa 32000, Israel.

[1]For a current survey, see *Surface Enhanced Raman Scattering,* edited by R. K. Chang and T. E. Furtak (Plenum, New York, 1982).

[2]H. J. Simon, D. E. Mitchell, and J. G. Watson, Phys. Rev. Lett. **33**, 1531 (1974).

[3]C. K. Chen, A. R. B. de Castro, and Y. R. Shen, Phys. Rev. Lett. **46**, 145 (1981).

[4]A. Wokaun, J. G. Bergman, J. P. Heritage, A. M. Glass, P. F. Liao, and D. H. Olson, Phys. Rev. B **24**, 849 (1981).

[5]C. K. Chen, T. F. Heinz, D. Ricard, and Y. R. Shen, Phys. Rev. B **27**, 1965 (1983).

[6]H. W. K. Tom, C. K. Chen, A. R. B. de Castro, and Y. R. Shen, Solid State Commun. **41**, 259 (1982).

[7]Y. J. Chen and E. Burstein, in *Surface Polaritons,* edited by V. M. Agronovich and D. L. Mills (North-Holland, Amsterdam, 1982).

[8]A. Otto, Z. Phys. **216**, 398 (1968).

[9]E. Kretschmann, Z. Phys. **241**, 313 (1971).

[10]H. J. Simon, D. E. Mitchell, and J. G. Watson, Am. J. Phys. **43**, 630 (1975).

[11]M. Fukui, O. Toda, V. C. Y. So, and G. I. Stegeman, Solid State Commun. **36**, 995 (1980); J. Phys. C **14**, 5591 (1981).

[12]H. Talaat, W. P. Chen, E. Burstein, and J. Schoenwald, in *Proceedings of the 1975 IEEE Ultrasonic Symposium* (IEEE, New York, 1975), p. 441.

[13]H. Talaat, W. P. Chen, and E. Burstein, J. Phys. C **15**, 3261 (1982).

[14]A. Marvin, V. Bortolani, F. Nizzoli, G. Santoro, and V. Celli, J. Phys. C **15**, 3273 (1982).

[15]J. R. Sandercock, Phys. Rev. Lett. **28**, 237 (1972); **29**, 1735 (1972).

[16]S. Mishra and R. Bray, Phys. Rev. Lett. **39**, 222 (1977).

[17]R. Loudon, Phys. Rev. Lett. **40**, 581 (1978).

[18]R. Loudon and J. R. Sandercock, J. Phys. C **13**, 2609 (1980).

[19]W. Knoll, M. R. Philpott, J. D. Swalen, and A. Girlando, J. Chem. Phys. **77**, 2254 (1982); Y. J. Chen, E. S. Koteles, R. J. Seymour, G. J. Sonek, and J. M. Ballantyne, Solid State Commun. **46**, 95 (1983).

[20]H. Raether, in *Surface Polaritons*, edited by V. M. Agronovich and D. L. Mills (North-Holland, Amsterdam, 1982).

[21]A. J. Braundmeier, Jr. and H. E. Tomaschke, Opt. Commun. **14**, 99 (1975).

[22]H. J. Simon and J. K. Guha, Opt. Commun. **18**, 391 (1976).

[23]J. R. Sandercock, in *Proceedings of the Second International Conference on Light Scattering in Solids, Paris, 1971*, edited by M. Balkanski (Flammarion Sciences, Paris, 1971).

[24]The use of a hemisphere, rather than a prism or cylinder, greatly expedited the performance of the experiments. We gratefully acknowledge a suggestion by A. Overhauser for making glass hemispheres very simply: the end of a Pyrex rod is melted, forming a nearly spherical solid bulb when suspended and cooled upside down. This is then cut into a hemispherical form, and the flat side is polished.

[25]V. Bortolani, F. Nizzoli, G. Santoro, J. R. Sandercock, and A. M. Marvin, in *Proceedings of the VIIth International Conference on Raman Spectroscopy, Ottawa, 1980,* edited by W. F. Murphy (North-Holland, Amsterdam, 1980).

[26]J. H. Weaver, C. Krafka, D. W. Lynch, and E. E. Koch, *Physics Data* (Fachinformationszentrum Energie, Physik, Mathematik GMBH, Karlsruhe, W. Germany, 1981), Vol. 2.

[27]It has been pointed out to us that very strong Raman scattering by the mechanical oscillations of metal islands (inelastic Mie scattering) has been observed. [See D. A. Weitz, T. J. Gramila, A. Z. Genack, and J. I. Gersten, Phys. Rev. Lett. **45**, 355 (1980); J. I. Gersten, D. A. Weitz, T. J. Garmila, and A. Z. Genack, Phys. Rev. B **22**, 4562 (1980)]. The very strong scattering was attributed to resonant interaction of the light with the localized plasmons of the Ag islands. The frequencies of the elastic vibrations (breathing modes of the particles) are related to the size and shape of the particles. Frequency shifts of about 300 GHz were observed, with half-widths of about the same magnitude. Our observation of an increased background in the Fabry-Perot scans is consistent with the presence of such strong, broad scattering contributions.